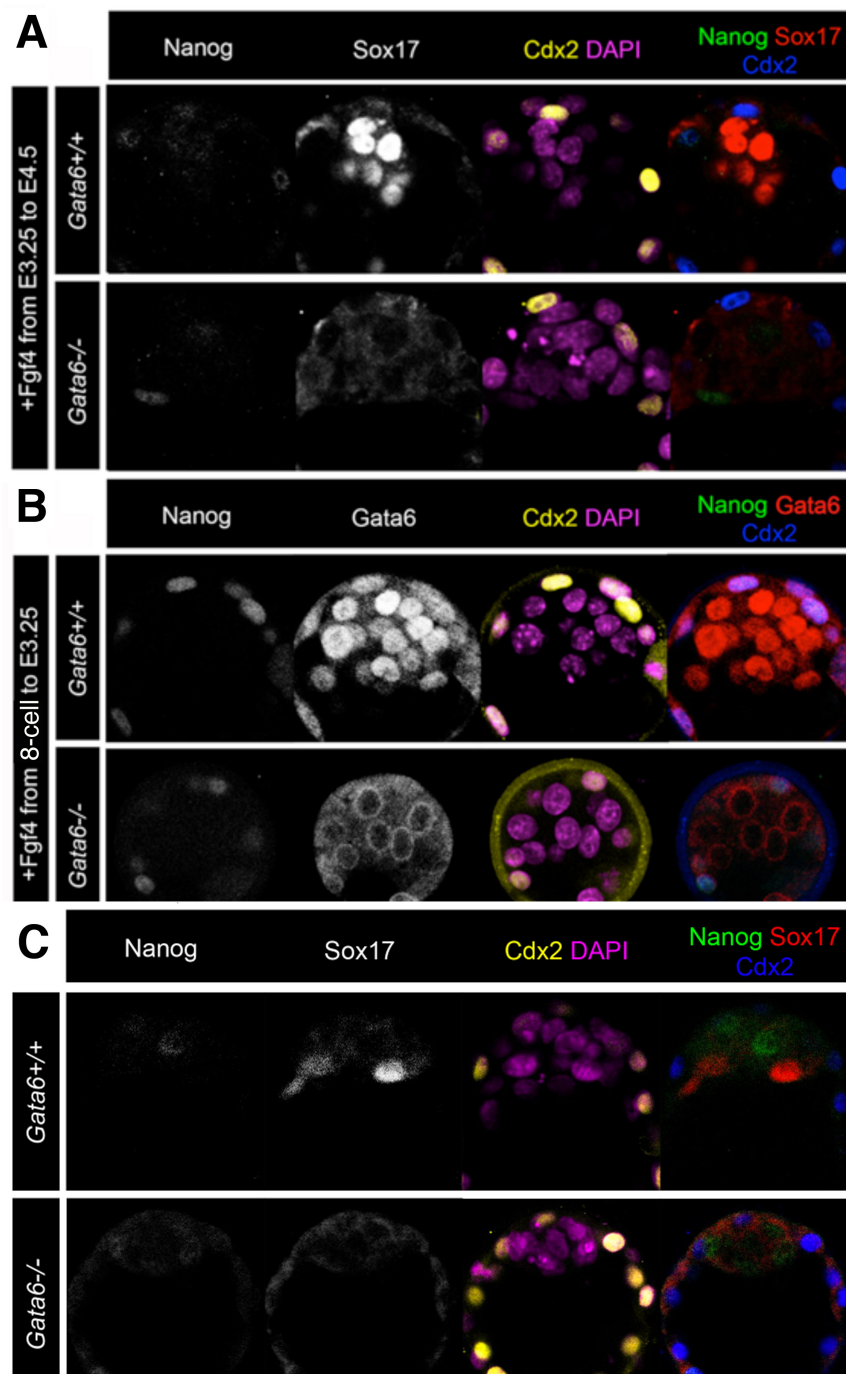**Gata6, Nanog and Erk Signaling Control Cell Fate in the Inner Cell Mass through a Tristable Regulatory Network**

S. Bessonnard, L. De Mot, D. Gonze, M. Barriol, C. Dennis, A. Goldbeter, G. Dupont and C. Chazaud.

SUPPLEMENTAL DATA

Figure S1 : Fgf4 treatment of WT and *Gata6*^{-/-} embryos cultured from E3.25 to E4.5 (WT: n=6; *Gata6*^{-/-}: n=7) **A.** and from the 8-cell stage to E3.25 (WT: n=3; *Gata6*^{-/-}: n=2) **B.** Embryos are immunolabeled to identify Epi, PrE and TE cells. C. Control embryo culture from E3.25 to E4.5 (WT: n= 10; *Gata6-/-*: n=7)
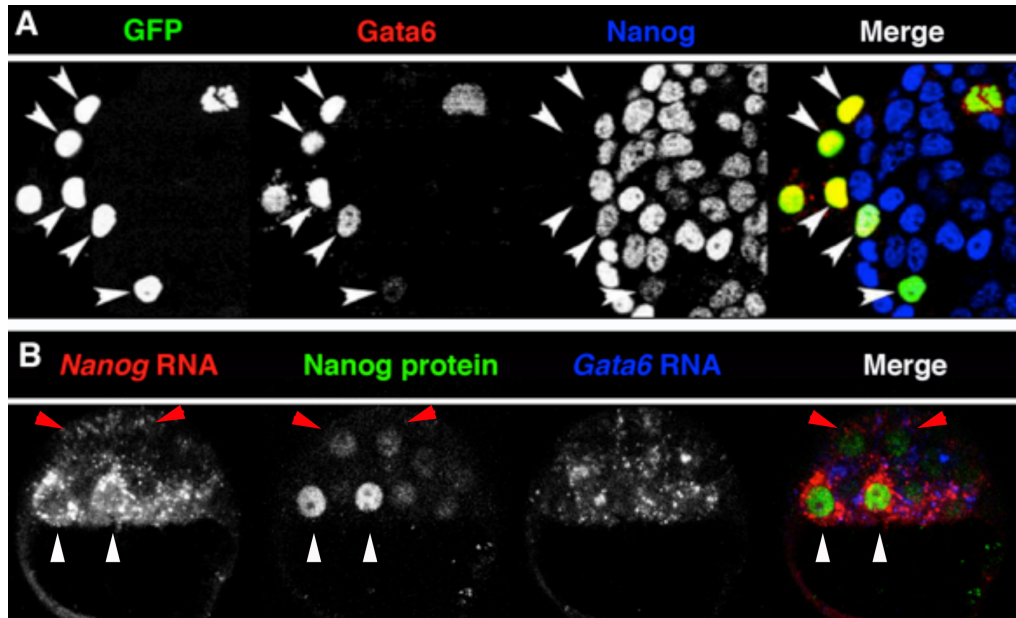

Figure S2: A. Under standard culture conditions (DMEM+ serum) F9 cells express high levels of Nanog with no Gata6 expression (not shown). In (**A**) F9 cells were transfected with a Gata6-2A-GFP pCAG expression plasmid in the presence of Fgfr+Mek inhibitors. Transfected cells are labelled by GFP; they express Gata6 and have downregulated Nanog expression cell-autonomously. Thus Gata6 can downregulate Nanog expression independently of the Fgf/RTK pathway. Arrowheads point toward some transfected cells. **B.** Double FISH targeting *Nanog* and *Gata6* mRNAs coupled with Nanog immunostaining at E3.5. *Nanog* RNAs and proteins colocalize to the same cells (see also Gasnier et al., 2013) and their low (red arrowheads), high (white arrowheads) levels are correlated as well as their absence of expression.
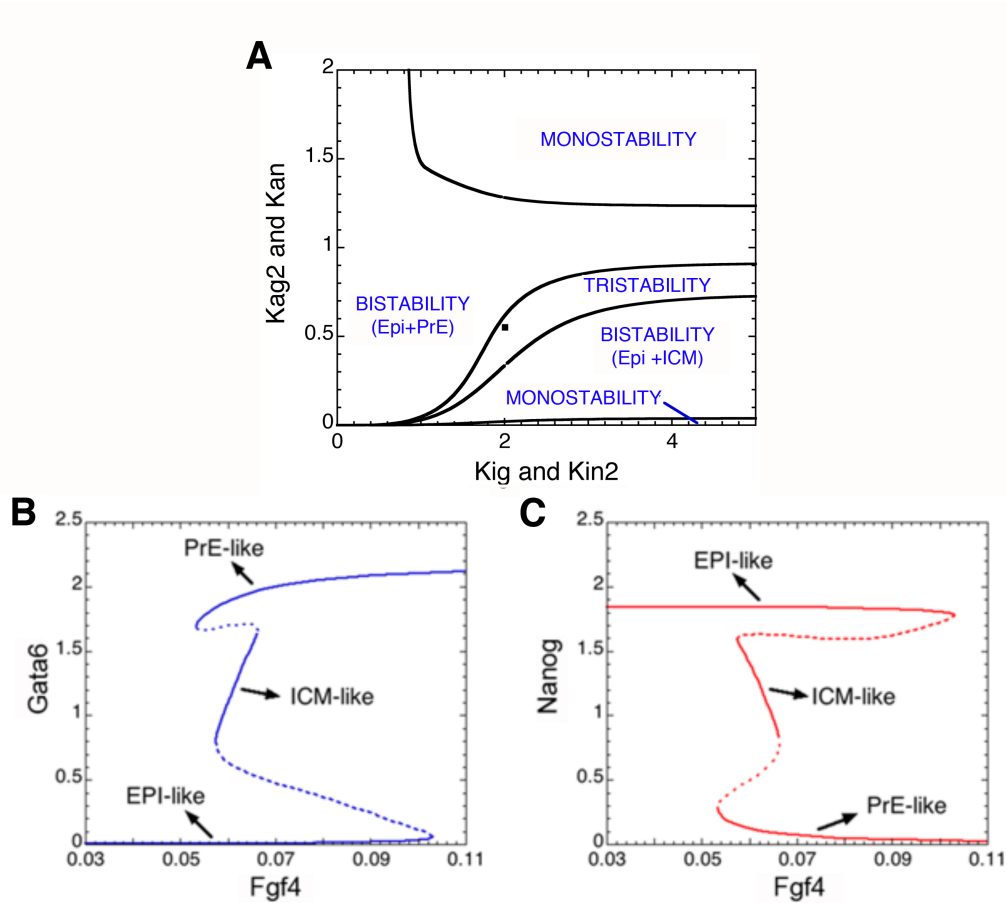
Figure S3 : Bifurcation diagrams obtained for a single cell-system defined by equations S1 to S4, with the concentration of Fgf4 (Fs) being treated as a parameter (see table S1 for parameter values). A. Domains of mono-, bi- and tristability in the (Kig and Kin2 taken as equal, Kag2 and Kan taken as equal) parameter space. B and C: These plots represent the stable (solid lines) and unstable (dashed lines) steady states of the model (presented in Figure 2 and defined by the four first equations (S1)-(S4) given in the Supplementary Materials and Methods) as a function of the extracellular concentration of Fgf4 perceived by the cell (*Fp*), for parameter values corresponding to the black square in panel A. The steady states are represented by the respective levels of (**B**) Gata6 or (**C**) Nanog. For 0.057<*Fp*<0.066, the system presents three stable steady states: an ICM-like state where both Nanog and Gata6 are expressed, an Epi-like state where only Nanog is expressed, and a PrE-like where only Gata6 is expressed. The Epi-like state is stable for *Fp*<0.103 whereas the PrE-like state is stable for *Fp*>0.053. In all panels, parameter values are given in table S1 unless specified. Panel A shows that, for the present choice of parameter values, tristability occurs for intermediate values of the auto-activation constants Kag2 and Kan, while for low and high values of these constants, the system evolves to a single steady state. The need for the auto-activation loops to generate tristability is further attested by the fact that the model no longer exhibits

3

tristability when Gata6 and Nanog self-activation loops are removed (*vsg2*=*vsn2*=0, not shown). The possibility nevertheless remains that even in such conditions tristability might occur for other parameter values, because of the multiplicity of remaining positive feedback loops in the network of regulatory interactions between Nanog, Gata6 and Erk signaling. The addition of exogenous Fgf4 corresponds to a large increase in the value of Fgf4 shown in abscissa, while the addition of ERK inhibitors corresponds to a large decrease in Fgf4 in the figures (B) and (C). The bifurcations diagrams in (A)-(C) have been obtained by means of the program AUTO (Doedel, 1981); see: http://indy.cs.concordia.ca/auto/#introduction.
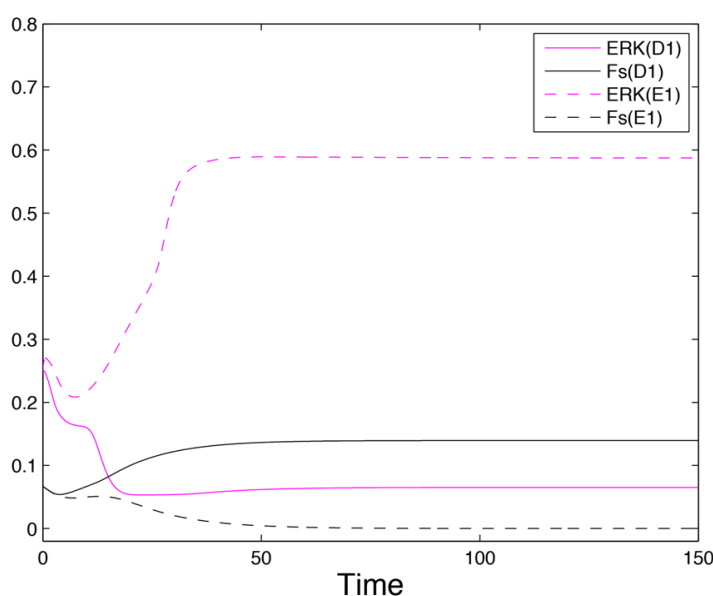

Figure S4 : Evolution of the relative activity of *ERK* and of the amount of Fgf4 produced by a WT cell differentiating into Epi (cell D1 in Figure 3A; solid curves) and by a WT cell adopting a PrE fate (cell E1 in Figure 3A; dashed curves). The initial level of *ERK* is high but it immediately decreases in both cells. Consequently, cell D1 differentiates in Epi and thus increases its production of Fgf4 (*Fs*). By contrast, *ERK* increases in cell E1, as a result of the Epi specification of its closest neighbors. Hence, this cell reaches the PrE-like state and stops synthesizing Fgf4. The units for time and concentrations are arbitrary. Parameter values are given in table S1. Initial conditions are: *G=N*=0, *FR*=2.8, *ERK*=0.25 and *Fs*=0.07.
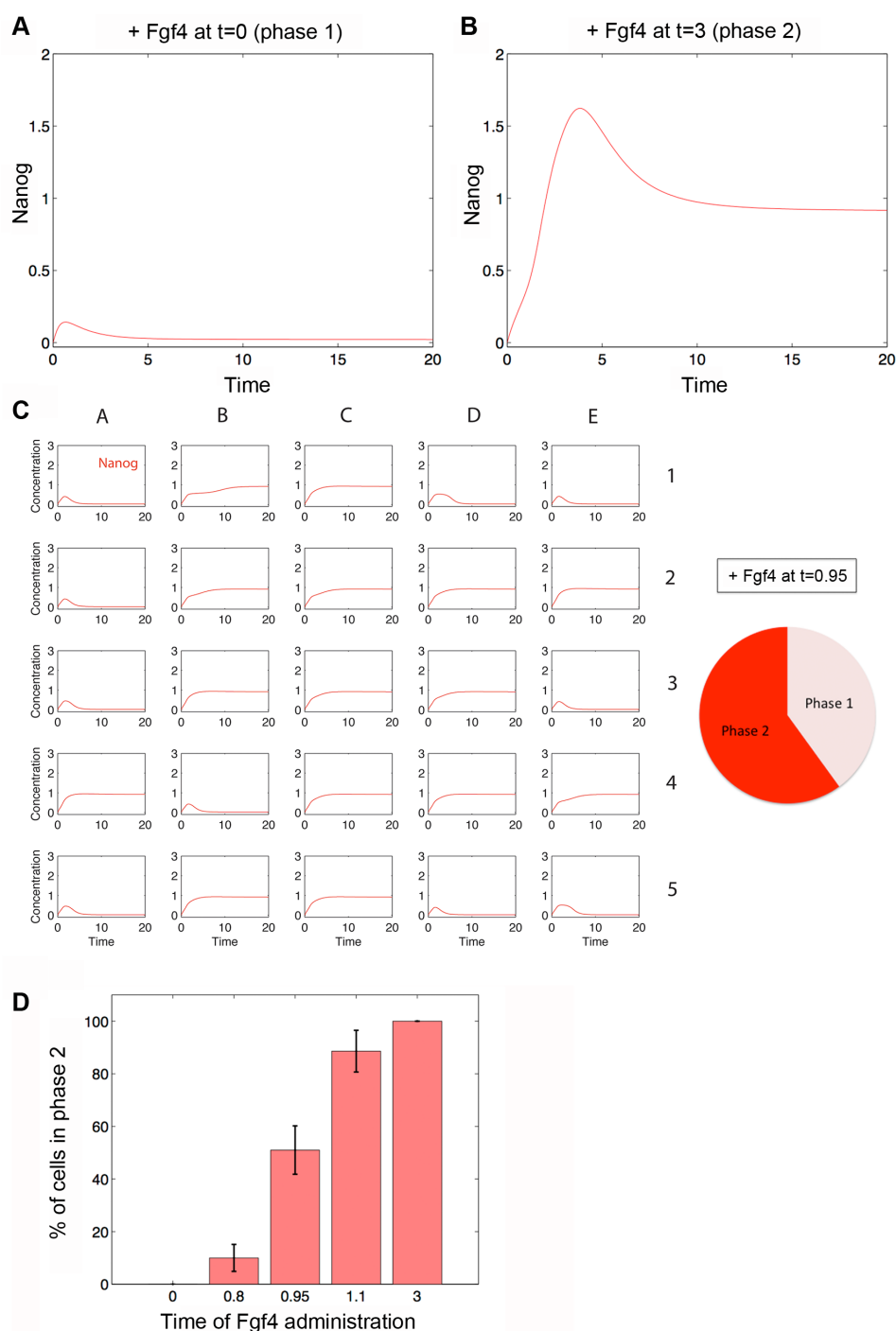
Figure S5 : Results obtained with the model for *Gata6*$^{-/-}$ cells treated with exogenous Fgf4. **A.** *Gata6*$^{-/-}$ cell treated with exogenous Fgf4 from the beginning of the simulation (t=0). In all the cells (only one is represented), Nanog remains low. Thus, all cells are still in phase 1. **B.** *Gata6*$^{-/-}$ cells treated with exogenous Fgf4 when Nanog is already at its maximal level (t=3). In all the cells (only one represented), Nanog is maintained. Thus, the cells are in phase 2. **C.** *Gata6*$^{-/-}$ cells treated with exogenous Fgf4 at t=0.95. Both behaviors are represented within the population. The pie chart shows the proportion of cells in phase 1 (10 cells) and in phase 2 (15 cells) for this simulation. In panels A-C, the red lines represent the concentrations of

Nanog. **D.** Proportion of *Gata6^(-/-)* cells maintaining Nanog expression, as a function of the time at which exogenous Fgf4 is administered**.** The later the treatment starts, the higher the proportion of these cells is. If Fgf4 is added at t=0.8, 10 (±5.3) % of the cells maintain Nanog expression. If the treatment starts at t=0.95, this proportion increases to 51 (±9.4) %. When Fgf4 is administered at t=1.1, the percentage of cells resisting to the treatment further increases to 88.6 (±8.1) %. The proportions have been computed using the results of 20 simulations of 25 cells in each condition. Both Gata6 and Nanog concentrations are null at t=0. In panels A-D, the units for time and concentrations are arbitrary. Parameter values are given in table S1. Initial conditions are: *G=N=0*, *FR=2.8*, *ERK=0.25* and *Fs=0.07*.
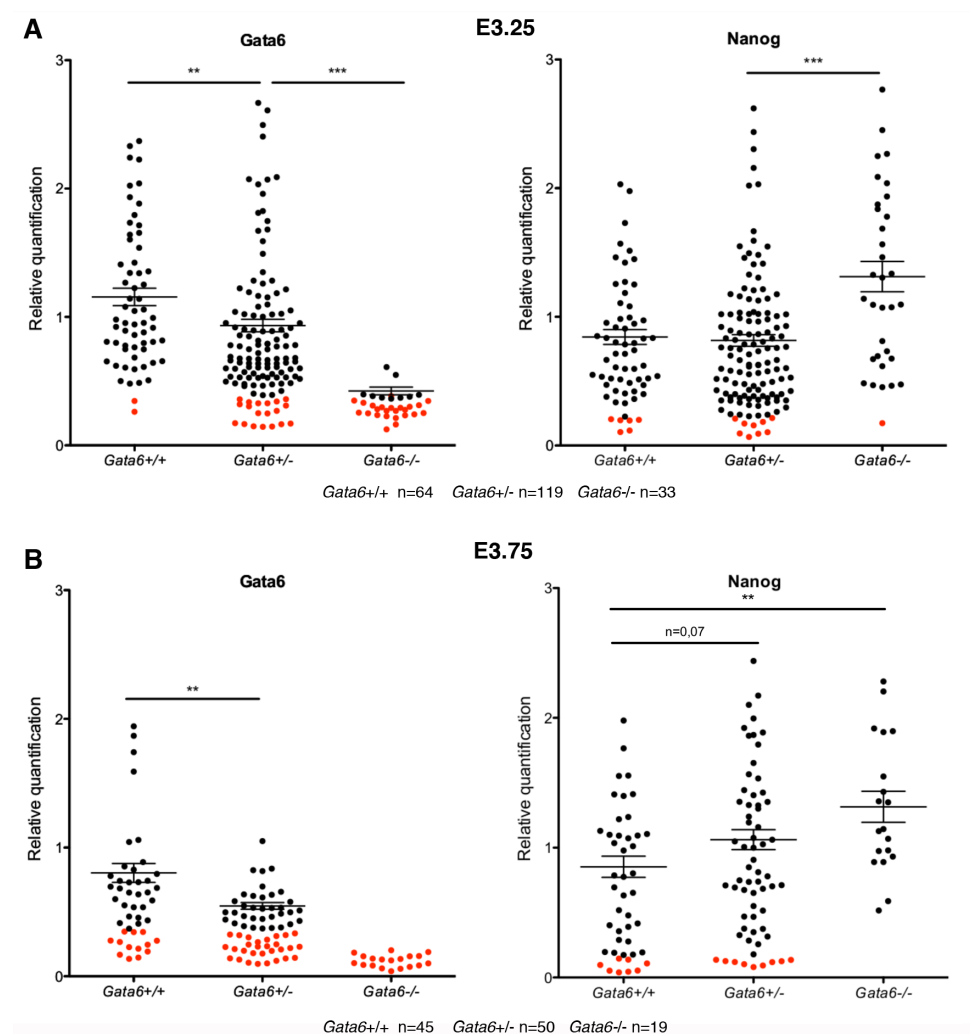
Figure S6 : Levels of Nanog and Gata6 in individual cells of WT, Gata6^(+/-) and Gata6^(-/-) embryos. The mean is represented by the horizontal bar (** p<0,01, *** p<0,001; Student test). Red dots represent values under the background level and are excluded in the calculation of the mean.

6
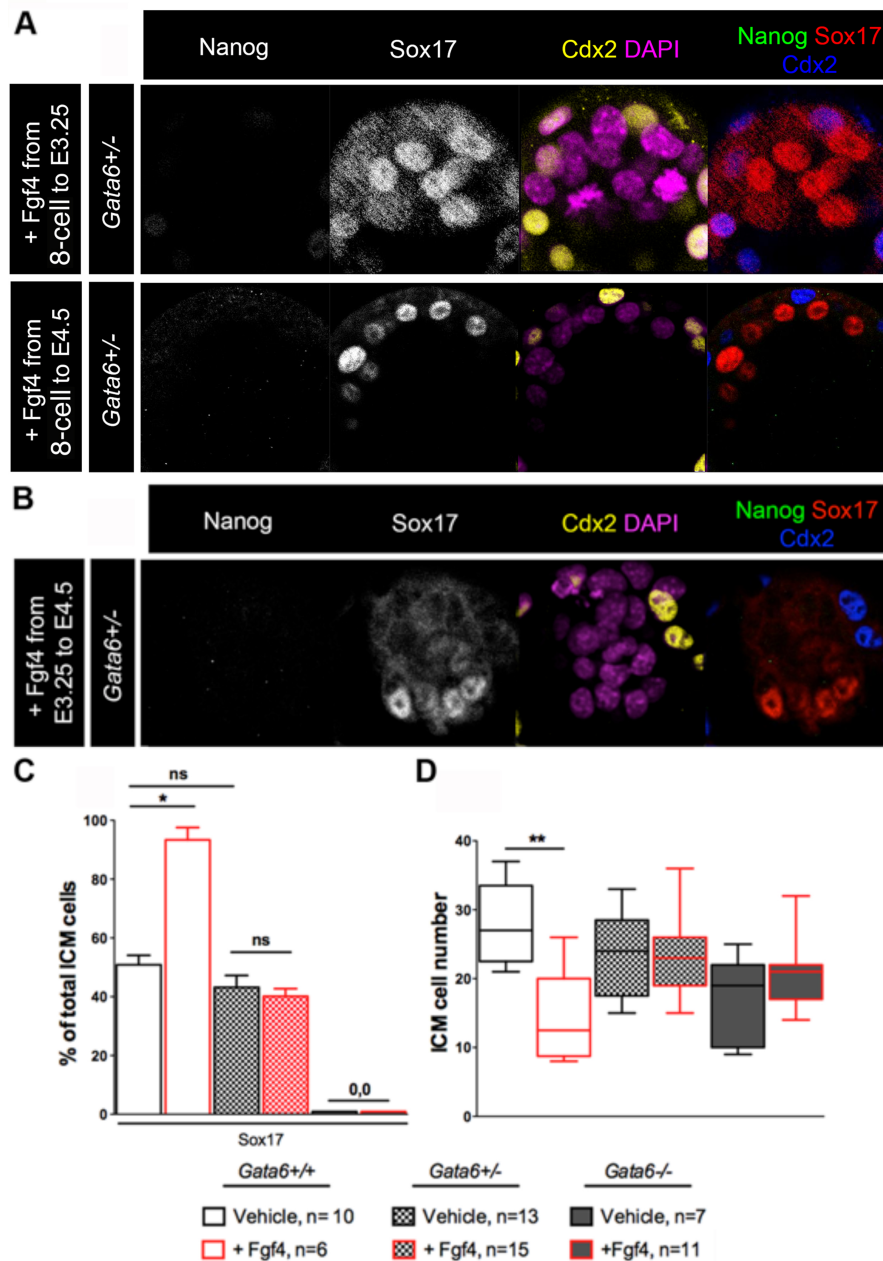
Figure S7 (related to Figure 6) **:** *Gata6*$^{+/-}$ embryos cultured with Fgf4. **A.** Cultures from the 8-cell stage to E3.25 (n=4) or from the 8-cell stage to E4.5 (n=4), immunolabeled with indicated markers. **B.** *Gata6*$^{+/-}$ embryos cultured in presence of Fgf4 from E3.25 to E4.5 (n=15). **C.** Percentage of Sox17-expressing cells in WT, *Gata6*$^{+/-}$ and *Gata6*$^{-/-}$ embryos after culture without or with Fgf4 from E3.25 to E4.5. **D.** Number of ICM cells after culture in both conditions. (* p<0,05, ** p<0,01; Mann-Whitney test, ns: non significant).

Name	Definition	Value
$vsg1$	Maximum rate of Gata6 synthesis caused by ERK activation	1.202 / 1.022 / 0 *
$vsg2$	Maximum rate of Gata6 synthesis caused by its auto-activation	1 / 0.85 / 0 *
$vsn1$	Basal rate of Nanog synthesis	0.856
$vsn2$	Maximum rate of Nanog synthesis caused by its auto-activation	1
$vsfr1$	Basal rate of Fgfr2 synthesis	2.8
$vsfr2$	Maximum rate of Fgfr2 synthesis caused by Gata6 activation	2.8
vex	Basal rate of Fgf4 synthesis	0 / 0.2 **
vsf	Maximum rate of Fgf4 synthesis caused by Nanog activation	0.6
va	ERK activation rate	20
vi	ERK inactivation rate	3.3
kdg	Gata6 degradation rate	1
kdn	Nanog degradation rate	1
$kdfr$	Fgfr2 degradation rate	1
kdf	Fgf4 degradation rate	0.077
$Kag1$	Threshold constant for the activation of Gata6 synthesis by ERK	0.28
$Kag2$	Threshold constant for Gata6 auto-activation	0.55
Kan	Threshold constant for Nanog auto-activation	0.55
$Kafr$	Threshold constant for the activation of Fgfr2 synthesis by Gata6	0.5
Kaf	Threshold constant for the activation of Fgf4 synthesis by Nanog	5
Kig	Threshold constant for the inhibition of Gata6 synthesis by Nanog	2
$Kin1$	Threshold constant for the inhibition of Nanog synthesis by ERK	0.28
$Kin2$	Threshold constant for the inhibition of Nanog synthesis by Gata6	2
$Kifr$	Threshold constant for the inhibition of Fgfr2 synthesis by Nanog	0.5
Ka	Michaelis constant for activation of the ERK pathway	0.7
Ki	Michaelis constant for inactivation of the ERK pathway	0.7
Kd	Michaelis constant for activation of the ERK pathway by Fgf4	2
r	Hill coefficient for the activation of Gata6 synthesis by ERK	3
s	Hill coefficient for Gata6 auto- activation	4
q	Hill coefficient for the inhibition of Gata6 synthesis by Nanog	4
u	Hill coefficient for the inhibition of Nanog synthesis by ERK	3
v	Hill coefficient for Nanog auto-activation	4
w	Hill coefficient for the inhibition of Nanog synthesis by Gata6	4
x	Hill coefficient for the inhibition of Fgfr2 synthesis by Nanog	1
y	Hill coefficient for the activation of Fgfr2 synthesis by Gata6	1
z	Hill coefficient for the activation of Fgf4 synthesis by Nanog	4

* WT / Gata6$^{+/-}$ / Gata6$^{-/-}$
** untreated / treated with exogenous Fgf4

Table S1 (related to Figure 2)**:** Parameter values used for numerical simulations of the model.

Supplementary Materials and Methods:

Gata6 mutant embryos genotyping and staging

Embryos were genotyped by PCR using the Goldstar Mix (Eurogentec) after the staining procedures. Primer Gata6WT-F: 5'-GTGGTTGTAAGGCGGTTTGT-3' was associated with Gata6Del-R: 5'-ACTTGGCAGAGATGAGGAAGGGA-3' to detect the mutant allele and with Gata6WT-R: 5'- TAATTCGTATAATGTATGCTATACGAAGTTAT-3' for the WT allele. Embryos were staged according to the time of their collection and their morphology: E2.75 (8-cell stage after compaction to 16-cell stage), E3.0 (16- to 32-cell stage), E3.25 (early expanding blastocyst), E3.5 (ICM volume equal to the cavity volume), E3.75 (ICM volume less than cavity volume, lineage precursors not fully sorted), E4.0 (sorted ICM; not implanted) and E4.5 (implanted, flat PrE epithelium; no parietal endoderm).

In situ labeling

Primary antibodies used in this study were Nanog (ab21603 and ab80892 -Abcam; RCAB0002P-F-Cosmo Bio), Gata6 (AF1700-R&D Systems), Sox17 (AF1924-R&D Systems), Gata4 (1237-Santa Cruz), Cdx2 (AM392-BioGenex). Secondary antibodies coupled with Alexa 488, Cy3 and Cy5 (Jackson ImmunoResearch) were used and nuclei were stained with DAPI (Sigma-Aldrich). The TE marker Cdx2 was used to clearly distinguish between TE and ICM cells. Embryos were scanned with a Leica SP5 laser confocal microscope (X40 objective) and analyzed with ImageJ (NIH).

Mathematical modeling:

To analyze the interactions between Nanog, Gata6 and ERK signaling, we constructed a phenomenological model, which describes the evolution of the protein levels and incorporates transcriptional regulations. We aimed at developing a model based on physiologically verified, most plausible assumptions, and capable to account for experimental observations presented in (Yamanaka et al., 2010), (Frankenberg et al., 2011). The mathematical model is described, for each cell, by a system of 5 ordinary differential equations. Equations (S1), (S2), (S3) and (S5) describe the temporal evolution of the level of a protein: Gata6 (*G*), Nanog (*N*), Fgfr2 (*FR*) and Fgf4 (*Fs*). Equation (S4) describes the temporal evolution of the normalized

level of activity of the Fgfr2/Erk pathway (*ERK*). The equations incorporate regulatory interactions described by Hill equations. Such equations are widely used to represent cooperativity in enzyme kinetics (see Hofmeyr and Cornish-Bowden, Comput. Appl. Biosci. 13, 377-85 (1997) for a critical discussion of the use of this expression in the context of metabolic pathways) and also to phenomenologically describe the binding of transcription factors (Alon, 2006). Equations of the Hill type have been utilized in the study of multistability and oscillations in a variety of metabolic and genetic regulatory networks.

In eq. (S1), Gata6 expression is activated by *ERK* and Gata6, and inhibited by Nanog; in eq. (S2), Nanog expression is inhibited by *ERK* and Gata6, and activated by itself; in eq. (S3), Fgfr2 expression is repressed by Nanog and induced by Gata6; in eq. (S5) Fgf4 synthesis is activated by Nanog, while *vex* denotes a basal rate of Fgf4 synthesis in the absence of Nanog. The equations for G, N, FR, and Fs all include a linear term of decay.

In our phenomenological approach, the choice between multiplicative or additive terms was made on the basis of a qualitative reasoning. Thus, in eq. (S1), inhibition by Nanog appears as multiplicative to prevent any increase of Gata6 in the presence of high levels of Nanog. In contrast, auto-activation and activation by the Erk pathway can both independently stimulate Gata6 synthesis. In the same manner, in eq. (S2), inhibition by Gata6 appears as multiplicative to prevent any increase of Nanog in the presence of high level of Gata6; inhibition by the Erk pathway is assumed to affect the synthesis of Nanog, which is independent of auto-activation. In Eq. (S3), we assume that Fgfr2 expression is repressed by Nanog and induced by Gata6 in an independent manner. In eq. (S4), the Erk pathway is compacted so that its activity (*ERK*) can be reversibly activated, with the rate of activation being proportional to both the fraction of receptor occupied by Fgf and the instantaneous amount of active Fgf4 receptors, Fgfr2 (*FR*); the rates of enzymatic activation and inactivation are of Michaelian form. As to secretion of Fgf4 (eq. (S5)), we consider both a basal and a Nanog-activated term.

(S1) to (S5)

$$\frac{dG}{dt} = \left[\frac{vsg1 \cdot ERK^r}{Kag1^r + ERK^r} + \frac{vsg2 \cdot G^s}{Kag2^s + G^s} \right] \cdot \frac{Kig^q}{Kig^q + N^q} - kdg \cdot G$$

$$\frac{dN}{dt} = \left[\frac{vsn1 \cdot Kin1^u}{Kin1^u + ERK^u} + \frac{vsn2 \cdot N^v}{Kan^v + N^v} \right] \cdot \frac{Kin2^w}{Kin2^w + G^w} - kdn \cdot N$$

$$\frac{dFR}{dt} = vsfr1 \cdot \frac{Kifr^x}{Kifr^x + N^x} + vsfr2 \cdot \frac{G^y}{Kafr^y + G^y} - kdfr \cdot FR$$

$$\frac{dERK}{dt} = va \cdot FR \cdot \frac{Fp}{Kd + Fp} \cdot \frac{1 - ERK}{Ka + 1 - ERK} - vi \cdot \frac{ERK}{Ki + ERK}$$

$$\frac{dFs}{dt} = vex + vsf \cdot \frac{N^z}{Kaf^z + N^z} - kdf \cdot Fs$$

Fp_i is the concentration of Fgf4 perceived by cell i. This concentration depends on the rate at which its four closest neighbors secrete Fgf4 :

(S6)

$$Fp_i = (1 + \gamma_i) \cdot \frac{\left(Fs_i + \sum_{j=1}^{4} Fs_{ij} \right)}{5}$$

where γ_i is a random number with a uniform distribution in the [-0.1, +0.1] interval (Figure 2), and where subscripts ij indicate the j nearest neighbors of cell i. Thus, the role of noise is expressed through parameter γ_i that accounts for the existence of slight inhomogeneities in the concentration of extracellular Fgf4: the concentration of this compound around a given cell is thus not given exactly by the average of the Fgf4 secreted by this cell and its closest neighbours. Instead, it is given by this average value increased or decreased by a few percents (γ_i). These inhomogeneities are due to the high level of compaction in the embryo: because cells are very close to one another, they act as barriers hindering the diffusion of extracellular compounds. Similar results are obtained when considering 8 neighbors instead if 4 in eq. (S6). In all simulations, boundary conditions are periodic. Parameter values are given in table S1. They were chosen phenomenologically in order for the model to account for the available experimental data —in particular those presented in (Yamanaka et al., 2010), (Frankenberg et al., 2011) and in this paper— on the proportions of ICM cells differentiating into PrE or Epi cells from wild-type and mutant embryos in a variety of conditions.

11

Initial conditions are given in the legend to Figure 3. For a given set of initial conditions and values of γ_i's, the same specification pattern will always emerge as simulations are totally deterministic. Because the γ_i are chosen randomly for each cell at the beginning of the simulation and kept constant during the whole simulation, a salt and pepper pattern will be obtained. Another random choice of γ_i's will produce a different pattern, which will, however, still be of the salt and pepper type. This fits with the observation that Epi and PrE cells are not positioned identically, as can be observed in vivo.

Estimation of the time required for a *Gata6$^{+/-}$* epiblastic cell to become irreversibly committed to its fate:

In WT and *Gata6$^{+/-}$* embryos, the Epi progenitors eventually become insensitive to exogenous Fgf4, respectively at E4.0 and 3.25, because of the activation of mechanisms of maturation that are not included in our model. Thus, at this stage, the Epi cells are irreversibly committed to the Epi fate. In this section, we estimate the time (in the model) at which a *Gata6$^{+/-}$* epiblastic cell should be considered as irreversibly committed.

In the WT embryo, all the ICM cells have differentiated in Epi or PrE by E3.75. In the model for a population of 25 WT cells, the last cells to differentiate are PrE cells, and they do so around 30–35 time units (WT populations). From this, we can assume that t=30 in the model roughly corresponds to E3.75 in the embryo.

In *Gata6$^{+/-}$* embryos, the epiblastic cells are irreversibly committed at E3.25 (Figure 6B). We do not know what the model-equivalent of E3.25 is, but we know that it is lower than t=30 (since t=30 corresponds to E3.75). Thus, in the simulations, the cells that reach the Epi-like state at the beginning of the simulations and remain in this state until t=30 (at least) are considered as epiblastic. In Figure 4D, for example, cells C3 and D4 are counted as epiblastic although they switch to the PrE-like state around t=40 / t=50. This behaviour is exhibited by 7.4% of the *Gata6$^{+/-}$* cells in average, but never occurs in the WT populations.

References :

Alon, U. (2006) *An Introduction to Systems Biology: Design Principles of Biological Circuits*, Chapman & Hall, CRC.

Doedel, E.J. (1981) 'AUTO: a program for the automatic bifurcation analysis of autonomous systems', *Congr. Numer.* 30: 265–284.

Frankenberg, S., Gerbe, F., Bessonnard, S., Belville, C., Pouchin, P., Bardot, O. and Chazaud, C. (2011) 'Primitive Endoderm Differentiates via a Three-Step Mechanism Involving Nanog and RTK Signaling', *Developmental cell* 21(6): 1005-13.

Gasnier, M., Dennis, C., Vaurs-Barriere, C. and Chazaud, C. (2013) 'Fluorescent mRNA labeling through cytoplasmic FISH', *Nature protocols* 8(12): 2538-2547.

Hofmeyr, J.H. and Cornish-Bowden, A. (1997) 'The reversible Hill equation: how to incorporate cooperative enzymes into metabolic models', *Comput. Appl. Biosci.* 13 (4):377-85.

Yamanaka, Y., Lanner, F. and Rossant, J. (2010) 'FGF signal-dependent segregation of primitive endoderm and epiblast in the mouse blastocyst', *Development* 137(5): 715-24.